UNIVERSITAT POLITÈCNICA
DE CATALUNYA

GEOPLEX: Control and Analysis of GSSA and VSS Models

C. Batlle, D. Biel, E. Fossas, C. Gaviria, and R. Griñó

IOC-DT-P-2004-20
Octubre 2004

Institut d'Organització i Control
de Sistemes Industrials

Control and Analysis of GSSA and VSS Models

C. Batlle[1,2,5], D. Biel[1,4], E. Fossas[3,5], C. Gaviria[5], and R. Griñó[3,5]
[1]EPSEVG, [2]MAIV, [3]ESAII, [4]EE, and [5]IOC
Technical University of Catalonia

July, 2004

Executive Summary

Two studies about a full-bridge boost rectifier are reported in this deliverable. In the first one the converter is analyzed in the frame of Variable Structure Systems and Sliding Mode. In the section 2 of the deliverable, the converter is analyzed in the frame of PCHS and controlled using IDA-PBC. The later includes experimental results.

The results reported here for both approaches can be generalized to several plants. The particularization to the full-bridge boost rectifier is natural, as this converter is supposed to be used in the Flywheel system to feed the rotor of the DFIM.

Section 1 studies the dynamics of a single-phase unity power factor full-bridge boost converter circuit and develops a nonlinear controller for the regulation of its output DC voltage, which keeps the input power factor close to unity. The controller has a two loop structure: the inner is a fast dynamic response loop with a sliding controller shaping the inductor input current of the converter, and the outer is a linear controlled slow dynamic response loop that regulates the output DC voltage. The squared value of the DC voltage is passed through a LTI notch filter to eliminate its ripple before using it in the outer control loop. This filter, consequently, allows one to expand the bandwidth of the loop and improves its dynamic response.

An Interconnection and Damping Assignment Passivity Based Control (IDA-PBC) for a full-bridge rectifier is presented in Section 2. The closed loop system performance fulfils unity power factor in the AC mains and output DC voltage regulation. The controller design takes advantage of the Generalized State Space Averaging (GSSA) modelling technique to convert the quoted non-standard problem (in actual variables) into a standard regulation one (in GSSA variables). In this approach, the output current is the measured signal instead of the line current; therefore, the number of sensors does not increase in comparison with traditional approaches. The whole system is robust with respect to load variations.

Contents

1 Sliding mode control of a full-bridge unity power factor rectifier

This section studies the dynamics of a single-phase unity power factor full-bridge boost converter circuit and develops a nonlinear controller for the regulation of its output DC voltage, which keeps the input power factor close to unity. The controller has a two loop structure: the inner is a fast dynamic response loop with a sliding controller shaping the inductor input current of the converter, and the outer is a linear controlled slow dynamic response loop that regulates the output DC voltage. The squared value of the DC voltage is passed through a LTI notch filter to eliminate its ripple before using it in the outer control loop. This filter, consequently, allows one to expand the bandwidth of the loop and improves its dynamic response.

1.1 Introduction

In order to meet the requirements of the electrical quality standards (for example IEC 1000-3-2) for the input current of low-power equipment, it is necessary to perform the AC-DC conversion of the electrical power using switch-mode power converters [9]. Among these circuits, the most popular choice for medium and high power applications is the boost power converter operating in continuous conduction mode [1, 16]. However, as it is known, it is difficult to control these converters because of their non-minimum phase behaviour with respect to the output voltage. This fact is worsened by the basic control objective of the sinusoidal shape in the converter input current. This specification has a non-standard form because it only imposes the shape of a signal and not its value as a function of time, which would fit to a tracking problem. Also, there is another control objective: the mean value of the DC bus capacitor voltage must be regulated to a specified value. But, as it will be seen in the next section, the two control objectives must accomplished with only one control variable, and this fact implies a complex controller structure, in general, a two control loop topology.

The section is organized as follows: Subsection II presents the model of the bidirectional boost rectifier and the control objectives. Subsection III discusses the steady-state and the zero-dynamics behaviour of the system, showing the converter input-output active power balance. Subsection IV develops a set of bounds for the system's response based on the physical parameters of the system. Subsection V shows the design of the controller detailing each one of the two loops (current and voltage). In Subsection VI several simulations of the proposed control scheme are showed. Finally, Subsection VII summarizes the conclusions.

1.2 Problem formulation

1.2.1 Physical model of the boost converter

The averaged model of the boost converter (at the switching frequency) [4] is given by

$$L\dot{x}_1 = -ux_2 - rx_1 + v_s \tag{1}$$

$$C\dot{x}_2 = ux_1 - \frac{1}{R}x_2 \tag{2}$$

where x_1 and x_2 are the input inductor current and the output capacitor voltage variables, respectively; $v_s = E\sin(\omega_r t)$ is the ideal sinusoidal source that represents the AC-line source; R is the DC-side resistive load; r is the parasitic resistance of the inductor; and L and C are the inductance and the capacitor of the converter. The control variable u takes its value in

the closed real interval $[-1, 1]$ and represents the averaged value of the PWM (pulse-width-modulated) control signal injected into the real system.

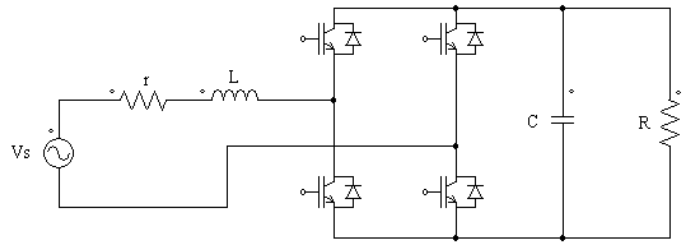

Figure 1: Bidirectional boost active rectifier converter.

In the actual implementation of the system it is assumed that the output voltage x_2, the input current x_1 and the source voltage v_s are available for measurement. In the following analysis, it will be interesting to deal with the DC component [1] of some variables that will be noted as $\langle\cdot\rangle_0$. It is important to remark that the system described by equations (1) and (2) can be seen as the interconnection of two subsystems with different time constants. In particular, the dynamics of equation (2) is much slower than the dynamics of equation (1). This fact has led to the development of the classical control schemes for these systems consisting of two concentric control loops: the inner (fast) for shaping the inductor current, and the outer (slow) for regulating the output capacitor voltage. In this control architecture, the output of the outer loop controller acts as the modulating signal in an AM modulator, with carrier v_s, whose output is the reference for the inner loop. The handicap of this control topology, caused by the slow outer voltage loop, is the need for big capacitors in the DC bus to prevent large overvoltages in case of great load perturbations.

1.3 Control objectives

The control objectives are:

1. The AC-DC converter must operate with a power factor close to one. This is achieved by ensuring that, in the steady-state, the inductor current x_1 follows a sinusoidal signal with the same frequency and phase as the AC-line voltage source v_s, i.e. $x_{1d} = I_d \sin(\omega_r t)$. The value for I_d should be calculated by the controller in order to accomplish the following objective,

2. The DC component of the output capacitor voltage $\langle x_2\rangle_0$ should be driven to the constant reference value $\langle x_2\rangle_{0d}$, where $\langle x_2\rangle_{0d} > E$ in order to have boost behaviour.

3. The value of the DC bus capacitor must be as low as possible for cost reasons. This requirement implies that the controller should be able to reject large perturbations in the load with short transients to prevent overvoltages in the bus.

1.4 Steady-State and Zero-Dynamics Analysis

If the state vector of the system (1)-(2) is fixed assuming perfect control action, at the desired values ($x_{1d} = I_d \sin(\omega_r t), x_{2d} = V_d = \langle x_2\rangle_{0d}$) and neglecting the higher order harmonics, an

[1] The DC component, or averaged function, of a periodic signal $f(t)$ of period T is calculated as $\langle f(t)\rangle_0 \triangleq \frac{1}{T}\int_{t-T}^{t} f(\tau)d\tau$.

input-output active power balance [4] is performed resulting in:

$$P_i = \langle x_{1d} v_s - r x_{1d}^2 \rangle_0 = \frac{1}{2}(E I_d - r I_d^2) \tag{3}$$

$$P_o = \frac{x_{2d}^2}{R} = \frac{V_d^2}{R} \tag{4}$$

Since the input active power must be equal to the output active power ($P_i = P_o$), then

$$\frac{1}{2}(E I_d - r I_d^2) = \frac{V_d^2}{R} \tag{5}$$

should hold. This equation has two solutions $I_d = \frac{E}{2r} \pm \sqrt{\frac{E^2}{4r^2} - \frac{2V_d^2}{rR}}$ which are real if and only if $\frac{V_d}{E} < \sqrt{\frac{R}{8r}}$ [4]. This condition is known as the boost condition of the power converter. The smaller solution of (5), $I_d = \frac{E}{2r} - \sqrt{\frac{E^2}{4r^2} - \frac{2V_d^2}{rR}}$, corresponds to a stable equilibrium and is the selected relation between the desired mean value of the DC capacitor (V_d) and the amplitude of the desired inductor current ($x_{1d} = I_d \sin(\omega_r t)$).

As it is known, the bidirectional boost rectifier has relative degree 1 regardless of the output, x_1 or x_2. Besides this, it is also known that if the output is x_2, the system has a non-minimum phase behaviour. For this reason, this system is usually controlled through the current x_1. In this case, the system has a minimum phase behaviour, i.e. its zero-dynamics is stable. In order to verify this assertion, x_1 is taken as the output of the system by fixing its value to $x_{1d} = I_d \sin(\omega_r t)$ in equations (1)-(2) resulting in

$$\overline{u} = \frac{(E - r I_d)\sin(\omega_r t) - \omega_r L I_d \cos(\omega_r t)}{\overline{x}_2} \tag{6}$$

$$\frac{d\overline{x}_2}{dt} = -\frac{{I_d}^2 \sin(\omega_r t)\cos(\omega_r t)\omega_r L}{C\overline{x}_2} - \frac{{I_d}^2 \left(\sin(\omega_r t)\right)^2 r}{C\overline{x}_2} + \frac{I_d \left(\sin(\omega_r t)\right)^2 E}{C\overline{x}_2} - \frac{\overline{x}_2}{CR} \tag{7}$$

where $\overline{u}$ and $\overline{x}_2$ are the control variable and the capacitor voltage, respectively, in the zero-dynamics. Then, equation (7) describes the behaviour of the zero-dynamics of the system. This equation is a Bernoulli ODE, but multiplying each side of the equation (7) by $\overline{x}_2$ and taking $\overline{z} = \frac{1}{2}\overline{x}_2^2$, we get the following linear ODE:

$$\frac{d\overline{z}}{dt} = -\frac{{I_d}^2 \sin(\omega_r t)\cos(\omega_r t)\omega_r L}{C} - \frac{{I_d}^2 \left(\sin(\omega_r t)\right)^2 r}{C} + \frac{I_d \left(\sin(\omega_r t)\right)^2 E}{C} - \frac{2\overline{z}}{CR}, \tag{8}$$

whose solution is $\overline{z}(t) = f(t) + p(t) + K$, where $f(t) = \frac{1}{2}C_1 \exp(-\frac{2t}{RC})$ is the vanishing ($\lim_{t\to\infty} f(t) = 0$) term corresponding to the first order linear dynamics, $p(t) = A\sin(2\omega_r t) + B\cos(2\omega_r t)$ is the oscillating term (at frequency $2\omega_r$), and $K = \frac{V_d^2}{2}$ is the constant term. It is worth noting that the DC value of $\overline{z}(t)$ in steady-state is $\langle \overline{z} \rangle_0 = K = \frac{V_d^2}{2}$, i.e. averaging $\overline{z}(t)$ with period $T = \frac{\pi}{\omega_r}$ in steady-state results in the mean value of the DC capacitor bus squared and divided by 2. The same result can be obtained averaging equation (8),

$$\frac{d\langle \overline{z} \rangle_0}{dt} = \frac{1}{2C}\left(E I_d - r I_d^2\right) - \frac{2\langle \overline{z} \rangle_0}{RC} = \frac{V_d^2}{RC} - \frac{2\langle \overline{z} \rangle_0}{RC} \tag{9}$$

whose solution is $\langle \overline{z} \rangle_0 = \frac{V_d^2}{2} + C_1 \exp(-\frac{2t}{RC})$.

1.5 Control Design

This section is devoted to the design of both the control u and I_d, since the latter operates as a control in a linear equation describing the dynamics of $\langle x_2^2/2 \rangle_0$. The control objectives can be

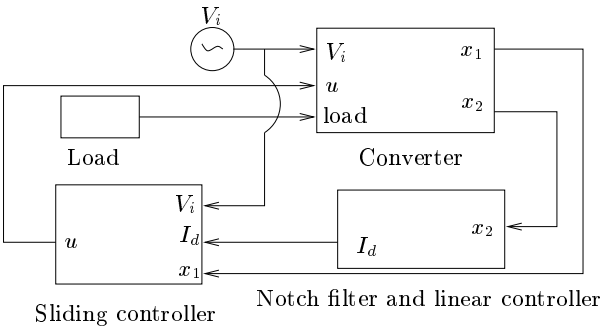

Figure 2: Control scheme blocks diagram.

written as follows:

- $x_1(t) = I_d \sin(\omega_r t)$
- $\langle z \rangle_0 = 0.5 V_g^2$

both requirements being demanded in steady-state, where $z = 0.5 x_2^2$.

As far as the first objective is concerned, sliding control is proposed since it is appropriate due to its very nature for switching converters, and it will provide a controlled system robust with respect to load variations [14]. Thus, $\sigma(x,t) = x_1 - I_d \sin(\omega_r t) = 0$ is considered as the switching surface. Note that its relative degree is one. Following the standard procedure [15], one has

$$u_{eq} = \frac{1}{x_2} \left[(E - rI_d) \sin(\omega_r t) - \omega_r L I_d \cos(\omega_r t) \right]$$

$$u = \begin{cases} -1 & \text{if } \sigma(x,t) < 0 \\ +1 & \text{if } \sigma(x,t) > 0 \end{cases}$$

A necessary condition for sliding motion is $x_2 \neq 0$; note that the dot product of the x-gradient of $\sigma(x,t)$ and the control vector is $-x_2/L$ which, in turn, will be assumed negative. Furthermore, $-1 \leqslant u_{eq}(x,t) \leqslant +1$ defines the subset of $\sigma(x,t) = 0$ where sliding motion occurs. The substitution of the zero-dynamics in these inequalities results in the necessary conditions to be held by the plant parameters and will be considered in the next section.

With regards to the second objective, the variable $\langle z \rangle_0$ is regulated to $V_d^2/2$ applying classical linear control design to equation (9) with $r = 0$, where I_d acts as the control variable. This ordinary differential equation describes the zero-dynamics, i.e. the Ideal Sliding Dynamics. Taking the zero-dynamics as the dynamics of $z = 0.5 x_2^2$ makes sense because the current loop is much faster than the voltage one, as has already been pointed out. In addition, $z(t)$ has a DC component and a fundamental harmonic at $2\omega_r$ which is removed through the linear notch filter

$$H(s) = \frac{s^2 + 4\omega_r^2}{s^2 + 4\xi\omega_r s + 4\omega_r^2} \tag{10}$$

A block diagram depicting this control scheme is shown in Fig. 2.

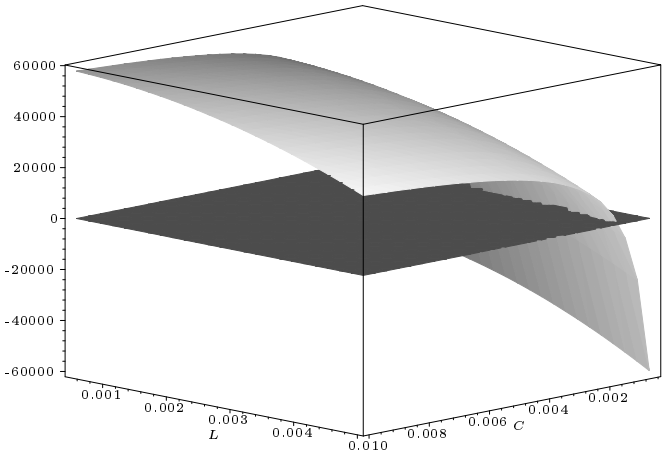

Figure 3: $\min^2\{d(t)\} - \max^2\{n(t)\}$ as a function of the variables (L, C) in the range $L \in [0.0005, 0.005]$, $C \in [0.0005, 0.01]$.

1.6 Parameter Analysis

The plant parameters are important in the performance of the controlled converter. Some of them, such as the load R and the input voltage, can vary with time, or can be affected by perturbations. Others, such as the inductance L and the capacitance C, are design parameters; that is to say, their values can be specified by the converter designer and can be assumed constant as long as the process takes. In this section, the influence of parameters L, C and R on the fulfilment of the control objectives is considered. Furthermore, a new specification is taken into account; namely, an output voltage ripple lower or equal to 0.05 p.u. For the sake of simplicity, $r = 0$ has been chosen in this section.

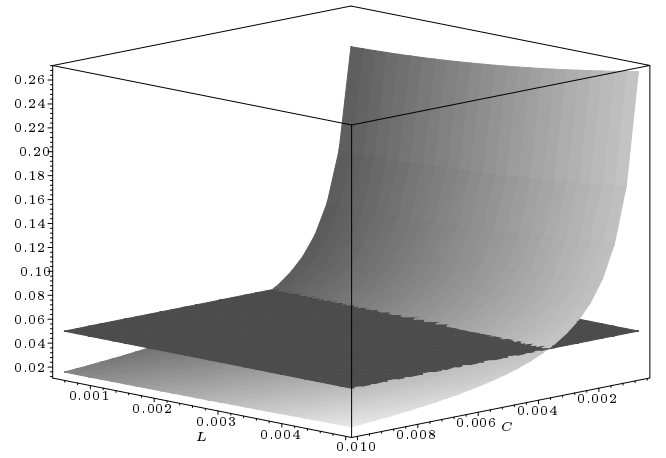

Figure 4: l_{pu} as a function of the variables (L, C) in the range $L \in [0.0005, 0.005]$, $C \in [0.0005, 0.01]$.

First, let it be assumed the steady-state for the input current, $x_1 = x_{1d} = I_d \sin(\omega_r t)$. From equation (1), the steady-state for the product ux_2 is given by

$$u_{ss}x_{2ss} = [E \sin(\omega_r t) - \omega_r L I_d \cos(\omega_r t)] \tag{11}$$

Second, as in the previous sections, the change of variable $z = 0.5x_2^2$ in equation (2) results

in

$$C\frac{dz}{dt} = ux_2x_1 - \frac{2z}{R} \tag{12}$$

Thus, from equations (11) and (12), the steady-state for the new variable z is

$$z_{ss}(t) = \frac{V_d^2}{2}\left[1 + \frac{2LCV_d^2\omega_r^2 - E^2}{E^2(1+\omega_r^2R^2C^2)}\cos(2\omega_r t) - \frac{\omega_r(E^2R^2C + 2LV_d^2)}{E^2R(1+\omega_r^2R^2C^2)}\sin(2\omega_r t)\right] \tag{13}$$

By substitution of $x_{2ss} = \sqrt{2z_{ss}}$ in equation (11), the steady-state for the input variable is obtained, which is a quotient of periodic signals. The numerator, $n(t)$, is a pure sine of amplitude

$$E\sqrt{1 + 4\frac{V_d^4\omega_r^2L^2}{E^4R^2}}$$

and the denominator, $d(t)$, is a periodic signal that oscillates between

$$V_d\sqrt{1 \pm \sqrt{\frac{\left(1 + 4\frac{\omega_r^2V_d^4L^2}{E^4R^2}\right)}{1+\omega_r^2R^2C^2}}}$$

A necessary condition to avoid saturation of the input variable, i.e. $0 < u < 1$, is

$$\max\{n(t)\} < \min\{d(t)\}$$

Since both terms of the inequality are positive, it is equivalent to

$$\begin{aligned}\min^2\{d(t)\} - \max^2\{n(t)\} &= V_d^2 - E^2\left(1 + 4\,\frac{\omega_r^2{V_d}^4L^2}{E^4R^2}\right) \\ &- \sqrt{V_d^4\left(1 + 4\,\frac{{\omega_r}^2{V_d}^4L^2}{E^4R^2}\right)(1+{\omega_r}^2R^2C^2)^{-1}} > 0\end{aligned} \tag{14}$$

Note that inequality (14) implies $V_d > E$, or equivalently, $\langle x_2\rangle_d > E$, recovering the boost character of this converter.

The graph of $\min^2\{d(t)\} - \max^2\{n(t)\}$ as a function of the variables (L, C) in the range $L \in [0.0005, 0.005]$, $C \in [0.0005, 0.01]$ is depicted in Fig. 3.

As for the second specification, from equation (13), the amplitude of the voltage ripple is given in **p.u.** by

$$l_{pu} = \sqrt{\left(1 + \sqrt{\frac{\left(E^4R^2 + 4\,{\omega_r}^2{V_d}^4L^2\right)}{E^4R^2\left(1+{\omega_r}^2R^2C^2\right)}}\right) - 1} \tag{15}$$

The graph of l_{pu} as a function of the variables (L, C) in the range $L \in [0.0005, 0.005]$, $C \in [0.0005, 0.01]$ is depicted in Fig. 4.

It is worth noting that if (14) and $l_{pu} < 0.05$ holds for L, C, E and R_0, it also holds for L, C, E and $R \geqslant R_0$. Both inequalities provide us with restrictions to be held by the parameters E,L, C, R, ω_r and V_d.

Comments

• From Figs. 3 and 4, $L \geqslant 0.001$ and $C \geqslant 0.003$ appear to be conditions for the specifications to be held, presuming $E = 220\sqrt{2}$V, $R_0 = 10\,\Omega$, $V_d = 400\,$V and $\omega_r = 100\pi\,$rad/s.

• Note from the pictures the dominance of the value of the capacitor in the fulfilment of the plant parameter requirements.

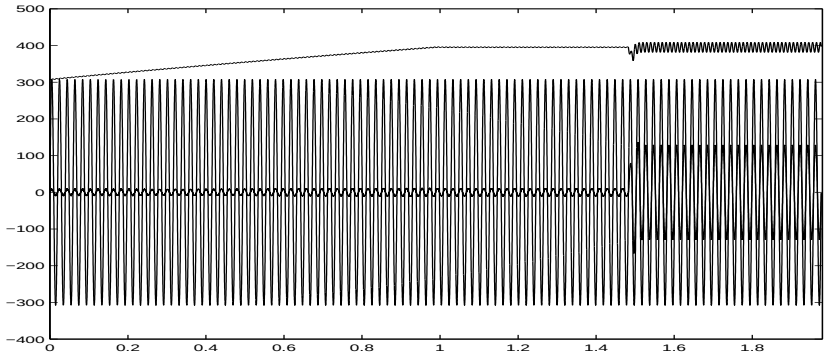

Figure 5: The input voltage $v_s(t)$ together with the input current $x_1(t)$ and the output voltage $x_2(t)$.

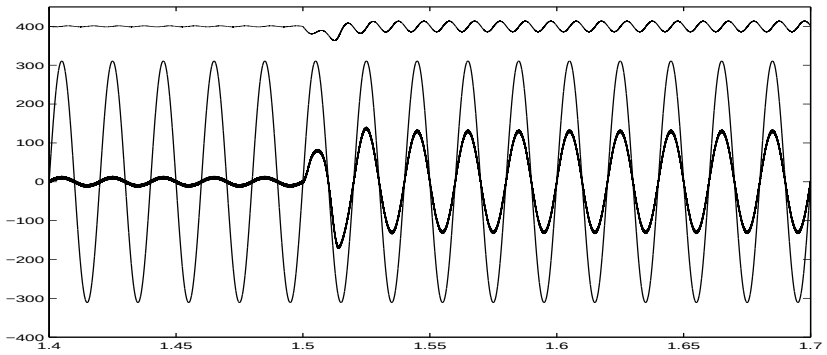

Figure 6: Input current $x_1(t)$ in phase with the input voltage $v_s(t)$.

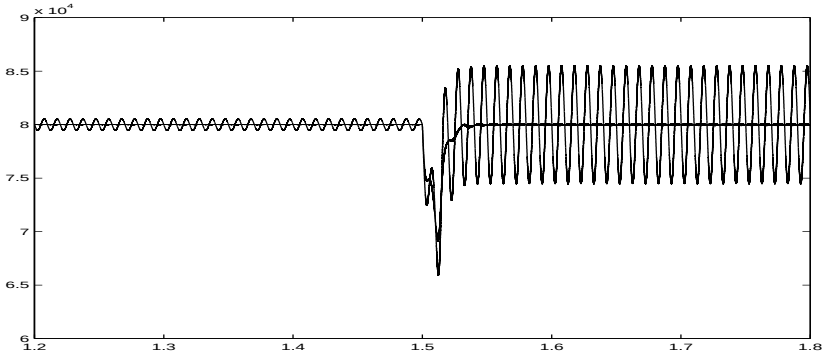

Figure 7: $z(t)$ together with $\langle z \rangle_0$.

1.7 Simulation results

The previous control design has been simulated in a single-phase active filter with the following parameters: $L = 1\,\text{mH}$, $C = 4.7\,\text{mF}$, $v_s(t) = 220\sqrt{2}\sin(\omega_r t)\,\text{V}$, $\omega_r = 100\pi\,\text{rad/s}$, $V_d = 400\,\text{V}$. A pulsating function taking values $R = 100\,\Omega$ and $R = 10\,\Omega$, respectively, has been considered as the resistive load. Fig. 5 shows the evolution of the input voltage v_s, the input current x_1 and the bus voltage x_2. A detail of the input current x_1 in phase with the output voltage v_s is shown in Fig. 6. Finally, in Fig. 7, the auxiliary variable $z = 0.5\,x_2^2$ is depicted together with the notch filter output, z being the input.

1.8 Conclusions

In this section, a dynamic sliding-mode control scheme for a single phase AC/DC regulator system with unity power factor has been proposed. The design procedure presented in this section suggests a sliding surface dynamically defined in order to fulfil two specifications in a single input system, namely: unity power factor and output voltage regulation. Fundamental to the regulation is a linear notch filter, eliminating the harmonics of the squared output voltage. A converter parameter design procedure that can be used to minimize the capacitor has also been proposed. The theoretical predictions have been validated by means of simulation results.

2 Robust Controller for a Full-Bridge Rectifier Using the IDA Approach and GSSA Modelling

An Interconnection and Damping Assignment Passivity Based Control (IDA-PBC) for a full-bridge rectifier is presented in this section. The closed loop system performance fulfils unity power factor in the AC mains and output DC voltage regulation. The controller design takes advantage of the Generalised State Space Averaging (GSSA) modelling technique to convert the quoted non-standard problem (in actual variables) into a standard regulation one (in GSSA variables). In this approach, the output current is the measured signal instead of the line current; therefore, the number of sensors does not increase in comparison with traditional approaches. The whole system is robust with respect to load variations.

2.1 Introduction

In industrial applications DC power supplies connected to AC mains must have some desirable properties such as high power density, high power factor, high efficiency, low current distortion, and simple control scheme, particularly due to the enforcement of strict harmonic regulations (for example IEC 61000-3-2) [7]. For medium and high power applications, the most popular choice to this end is the power switching boost rectifier operating in continuous conduction mode [5]. However, it is difficult to control these converters because of their non-minimum phase behaviour with respect to the output voltage, which, in turn, is worsened by the basic control objective of the sinusoidal shape in the converter line current. This specification has a non-standard form because it only imposes the shape of a signal and not its value as a function of time, which would pose to a tracking problem.

Using the GSSA [13] modelling method, it is possible to describe the control objectives, namely load voltage regulation and unity power factor at the input AC mains, as a regulation problem. Generally speaking, industrial loads for this rectifier are variable loads, this being the main drawback to obtain simple controllers. Common solutions require the sensing of input voltage, line current and output voltage. Achieving robustness to load variations is not a simple control problem because whenever load varies, the amplitude of the line current must change to a new value to keep DC voltage regulation, but keeping the control objective over the line current shape. It is difficult to treat this problem as a tracking problem without measuring the load since the line current reference depends on it.

As reported in the excellent survey [10], traditional control strategies establish two loops: an line current inner loop for power factor compensation and an output voltage outer loop for voltage regulation. Works [3] and [11] warn of difficulties in actual implementations of these two loops because of the different dynamics they undergo. An adaptive scheme, which results in a complex control law, is proposed in [4]. All of these works use at least two sensors; even three as an extra output current measure is required to estimate the load.

The control proposed here has been designed for a non linear GSSA model with an inherited Port Controlled Hamiltonian (PCH) structure. We take advantage of this structure to solve the aforementioned GSSA regulation problem and we obtain a closed-loop system robust to load variations. For this proposal, only two signals need to be measured, namely the output voltage and the output current, this being one of the main results of this section. The input voltage amplitude is supposed to be known, e.g. through sensing.

Interconnection and damping assignment passivity based control has been developed in the last years by Ortega et alt. as a control technique based on energy balance. It was applied solve regulation problems in physical systems written in Euler-Lagrange equations and recently ex-

tended to Port Controlled Hamiltonian Systems. The reader is referred to [12] and the references therein for basic results.

The main contributions of the present section are: first, a tracking problem is solved in a PCH framework; using GSSA models it is possible to transform the non-standard tracking control problem into a regulation one. Second, the extension of the Hamiltonian structure of the nonlinear model to the GSSA model and finally, the experimental validation of the control strategy designed.

The section is organised as follows. Second Subsection provides a short review of the GSSA modelling technique. The third Subsection develops a preliminary analysis of the system based on the energy in steady state and states the control objectives. In Subsection four a GSSA model for the full-bridge converter in its relevant harmonics is obtained and written as a PCH system. The fifth Subsection develops the IDA approach for this system to obtain a stabilising control law. The sixth Subsection shows simulation results obtained from a switched model of the full-bridge rectifier, and the robustness to load variations behaviour is remarked. The seventh Subsection describes the experimental setup and shows experimental results. Finally, some conclusions are drawn.

2.2 Review of the GSSA method

The GSSA method was introduced in [13] and expanded later to highlight the accuracy of this modelling technique applied to describe the dynamic behaviour of DC/DC converters in [8] and [2]. This review has been taken from the last reference.

The method is based on the fact that a signal $x(\tau)$ on the interval $\tau \in [t-T, t]$ can be represented by the Fourier series

$$x(\tau) = \sum_{\ell=-\infty}^{\infty} \langle x \rangle_\ell(t) e^{j\ell\omega_o\tau}, \tag{16}$$

where $\omega_o = 2\frac{\pi}{T}$ and $\langle x \rangle_\ell(t)$ are the time-dependent complex Fourier coefficients given by

$$\langle x \rangle_k(t) = \frac{1}{T}\int_{t-T}^{t} x(\tau) e^{-jk\omega_o\tau} d\tau. \tag{17}$$

To reconstruct $x(\tau)$ from its Fourier coefficients, equation (16) can be reformulated as

$$x(\tau) = \langle x \rangle_0 + 2\sum_{\ell=1}^{\infty} (\Re\langle x \rangle_\ell \cos(\ell\omega_o\tau) - \Im\langle x \rangle_\ell \sin(\ell\omega_o\tau)), \tag{18}$$

where the time argument t of $\langle x \rangle_\ell$ has been dropped to simplify the notation, and $\Re\langle x \rangle_\ell$ and $\Im\langle x \rangle_\ell$ are the real and imaginary parts of $\langle x \rangle_\ell$, respectively.

In order to use this representation for the $x(\tau)$ in a state-space model of a system, two useful facts concerning differentiation with respect to time and computation of the average of a product are

$$\frac{d\langle x \rangle_k(t)}{dt} = \langle \frac{dx}{dt} \rangle_k(t) - jk\omega_o \langle x \rangle_k(t) \tag{19}$$

$$\langle qx \rangle_k = \sum_{i=-\infty}^{\infty} \langle q \rangle_{k-i} \langle x \rangle_i. \tag{20}$$

PSfrag replacements

$\frac{\phi}{L}$
$\frac{q}{C}$
r
L
C
R
v_i
$+$
$-$

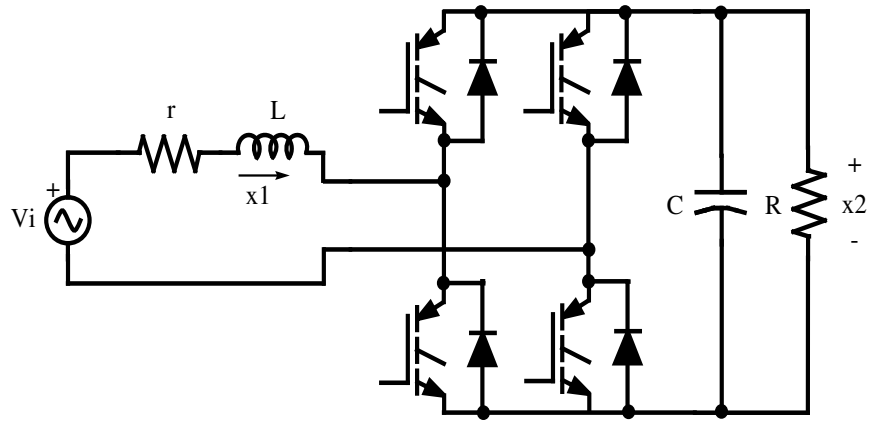

Figure 8: Full-bridge boost type rectifier

2.3 Preliminary analysis of the system

The following equations describe the dynamical behaviour of the full-bridge boost type rectifier in Fig. 8.

$$\frac{d\phi(t)}{dt} = \frac{-u(t)}{C}\, q(t) - \frac{r}{L}\phi(t) + v_i(t) \tag{21}$$

$$\frac{dq(t)}{dt} = \frac{u(t)}{L}\, \phi(t) - i_l(t) \tag{22}$$

where $\phi(t)$ is the magnetic flux through inductor L, $q(t)$ is the electrical charge in capacitor C, r is a resistance modelling the parasitic resistive effect of the inductor and the switches, $u(t)$ describes the position of the switches taking values in the discrete set $\{-1, 1\}$, $i_l(t)$ is the load current and $v_i(t) = E\sin(\omega_o t)$ is the AC voltage source of amplitude E and angular frequency $\omega_o = 2\pi f$, f being the frequency in Hz. In this section, and only for GSSA modelling purposes, the load will be assumed resistive, then $i_l = \frac{q}{C}\frac{1}{R}$.

As in [4], the control objectives for this rectifier are [2]

- The DC value of the output voltage $\frac{q(t)}{C}$, $\frac{\langle q(t)\rangle_0}{C}$ should be equal to a desired constant value $V_d > E$; i.e.

$$\langle q(t)\rangle_0{}^* = CV_d \tag{23}$$

- The power factor of the converter should be equal to one. This means that, in steady-state, the inductor current $\frac{\phi(t)}{L}$ follows a sinusoidal signal with the same frequency and phase as the AC-line voltage source; i.e.

$$\phi^*(t) = LI_d \sin(\omega_o t), \tag{24}$$

  where I_d is the appropriate constant value fulfilling the aforementioned objective.

Note that the second control objective does not correspond to a tracking problem because amplitude I_d depends on variable $i_l(t)$.

[2] In this paper * will be used to express the value in steady-state

A useful variable transformation which simplifies [3] forthcoming developments is obtained through $v(t) = -u(t)q(t)$ and $\mathbf{z} = [z_1, z_2] = [\phi(t), \frac{1}{2}q(t)^2]$. The system in the new variables is

$$\frac{dz_1(t)}{dt} = -\frac{rz_1(t)}{L} + \frac{v(t)}{C} + v_i(t) \tag{25}$$

$$\frac{dz_2(t)}{dt} = -\frac{v(t)z_1(t)}{L} - i_l(t)\sqrt{2\ z_2(t)}. \tag{26}$$

The energy in the storing elements L and C of this system can be described by

$$H_T(t) = \frac{z_1(t)^2}{2L} + \frac{z_2(t)}{C} \tag{27}$$

and equations (25-26) can be rewritten as

$$\begin{bmatrix} \frac{dz_1(t)}{dt} \\ \frac{dz_2(t)}{dt} \end{bmatrix} = \begin{bmatrix} 0 & v(t) \\ -v(t) & 0 \end{bmatrix} \frac{\partial H_T}{\partial \mathbf{z}} - \begin{bmatrix} r & 0 \\ 0 & Ci_l(t)\sqrt{2\ z_2(t)} \end{bmatrix} \frac{\partial H_T}{\partial \mathbf{z}} + \begin{bmatrix} v_i(t) \\ 0 \end{bmatrix}, \tag{28}$$

which corresponds to a PCHS system [12] of the form

$$\dot{\mathbf{z}} = [\mathbf{J}_T(\mathbf{v}) - \mathbf{R}_T(\mathbf{x})] \frac{\partial H_T}{\partial \mathbf{z}}(\mathbf{z}) + \mathbf{g}_T, \tag{29}$$

where $\mathbf{J}_T = -\mathbf{J}_T^T$, $\mathbf{R}_T(\mathbf{x}) = \mathbf{R}_T^T(\mathbf{x}) \geqslant 0$ are the matrices in equation (28) describing the interconnection structure and damping, respectively. The last inequality results from $z_2(t) \geqslant 0$ and $i_l(t) \geqslant 0$ because the load voltage is non negative. The input voltage $(v_i(t), 0)$ is considered as an external disturbance modelled by vector $\mathbf{g}_T$. In order to obtain the simplest coherent GSSA model, let us determine the harmonic content of the states and the input in steady-state.

To this end, let $z_1^*(t) = LI_d \sin(\omega_o t)$ be the z_1 desired dynamics and $i_l(t)$ the load current assuming a resistive load. In order to obtain the steady-state zero dynamics, let us take into account this assumption in equations (25-26) and let us solve for v and z_2. The steady state response yields

$$z_2^*(t) = \alpha_{z2} + \beta_{z2}\ \sin(2\omega_o t + \theta_{z2}) \tag{30}$$

$$v^*(t) = C(E - rI_d)\sin(\omega_o t) + I_d \omega_o LC \cos(\omega_o t), \tag{31}$$

where

$$\alpha_{z2} = \frac{I_d RC^2}{4}\ (E - rI_d)$$

$$\beta_{z2} = \frac{I_d RC^2}{4}\sqrt{\frac{(E - rI_d)^2 + (I_d \omega_o L)^2}{1 + (\omega_o RC)^2}}$$

$$\tan(\theta_{z2}) = \frac{(E - rI_d) - \omega_o RC(\omega_o LI_d)}{\omega_o RC(E - rI_d) + \omega_o LI_d}$$

The value of parameter I_d can be obtained from equation (23). Note that α_{z2} is the output voltage DC-component to be achieved. Thus, $\alpha_{z2} = \frac{C^2 V_d^2}{2}$, and

$$I_d = \frac{E}{2\ r} \mp \sqrt{\left(\frac{E}{2\ r}\right)^2 - \frac{2V_d^2}{rR}} \tag{32}$$

[3] First, the new input v linearises and decouples the first equation; second, the Fourier expansion of q^2 is much simpler than that of q, at least in steady-state.

As in [5] and [4] the expression for the I_d can also be obtained through power balance. The minus sign has been chosen since it yields a stable equilibrium point with lower power consumption. The total stored energy in steady-state results in

$$H_T^*(t) = \alpha_H + \beta_H \ \sin(2\omega_o t + \theta_H), \tag{33}$$

where

$$\begin{aligned} \alpha_H &= \frac{I_d CR}{4}(E - rI_d) + \frac{LI_d^2}{4} \\ \beta_H &= \frac{\frac{I_d CR}{4}(E - rI_d) + \frac{LI_d^2}{4}}{\sqrt{1 + (\omega_o RC)^2}} \\ \tan(\theta_H) &= \frac{1}{\omega_o RC}. \end{aligned}$$

Expressions (30), (31) and (24) show that a suitable GSSA model of the system, useful for controller design purposes, should contemplate the first harmonic Fourier components for $z_1(t)$, the zero and second harmonic Fourier components for $z_2(t)$ and the first harmonic Fourier components for $v(t)$. As for the Hamiltonian $H_T(t)$, from equation (33), the DC-component and second harmonic should be considered. If, in addition, C is chosen to obtain a low voltage ripple in the capacitor, then β_{z2} and β_H are negligible with respect to α_{z2} and α_H, respectively. Hence, the second harmonic Fourier components of $z_2(t)$ and $H_T(t)$ will not be considered from now on.

2.4 The Full-Bridge rectifier as a PCH system in GSSA variables

Although the most general GSSA model of a system has infinite dimension, the harmonic contents of signals in steady-state can be used to find accurately enough finite dimensional GSSA models. To this aim, using (20) and taking into account the Fourier components we have considered as relevant, the bilinear product $v(t)z_1(t)$ in (26) can be approximated as

$$\begin{aligned} \langle vz_1\rangle_0 &= \sum_{k=-\infty}^{\infty} \langle v\rangle_{-k}\langle z_1\rangle_k = \langle v\rangle_0\langle z_1\rangle_0 + 2\sum_{k=1}^{\infty}\left(\langle v\rangle_k^R\langle z_1\rangle_k^R + \langle v\rangle_k^I\langle z_1\rangle_k^I\right) \\ &\simeq 2\left(\langle v\rangle_1^R\langle z_1\rangle_1^R + \langle v\rangle_1^I\langle z_1\rangle_1^I\right). \end{aligned} \tag{34}$$

Furthermore,

$$\langle i_l q\rangle_0 \simeq \langle i_l\rangle_0\langle q\rangle_0 + 2\left(\langle i_l\rangle_1^R\langle q\rangle_1^R + \langle i_l\rangle_1^I\langle q\rangle_1^I\right) \tag{35}$$

As it has been assumed $q(t)$ has predominantly DC harmonic components, the complex coefficients of order one in equation (35) will be discarded. Thus, $\langle z_2\rangle_0 \simeq \frac{1}{2}(\langle q\rangle_0)^2$ and $\langle q\rangle_0 \simeq \sqrt{2\langle z_2\rangle_0}$. Hence, using equations (19), (34) and (35), the GSSA model of the system defined by (26) becomes

$$\begin{aligned} \frac{d\langle z_2\rangle_0}{dt} &= -\langle i_l\rangle_0\sqrt{2\langle z_2\rangle_0} - \frac{2}{L}\langle v\rangle_1^R\langle z_1\rangle_1^R - \frac{2}{L}\langle v\rangle_1^I\langle z_1\rangle_1^I \\ \frac{d\langle z_1\rangle_1^R}{dt} &= -\frac{r}{L}\langle z_1\rangle_1^R + \frac{1}{C}\langle v\rangle_1^R + \omega_o\langle z_1\rangle_1^I \\ \frac{d\langle z_1\rangle_1^I}{dt} &= -\frac{r}{L}\langle z_1\rangle_1^I + \frac{1}{C}\langle v\rangle_1^I - \omega_o\langle z_1\rangle_1^R - \frac{E}{2}. \end{aligned} \tag{36}$$

Let $\mathbf{x} = [\langle z_2\rangle_0, \langle z_1\rangle_1^R, \langle z_1\rangle_1^I]$, $\mathbf{u} = [\langle v\rangle_1^R, \langle v\rangle_1^I]$ be the state and control vectors, respectively, and

$$\mathbf{x}^* = \left[\frac{C^2V_d^2}{2}, 0, \frac{-LI_d}{2}\right] \tag{37}$$

the desired equilibrium.

The original control problem has become a regulation problem in the GSSA domain. For simplicity, let us denote the load current DC component by $I_o = \langle i_l\rangle_0$. Then, the system in (36) can be written as the PCH system:

$$\begin{bmatrix} \frac{dx_1(t)}{dt} \\ \frac{dx_2(t)}{dt} \\ \frac{dx_3(t)}{dt} \end{bmatrix} = \begin{bmatrix} 0 & -u_1 & -u_2 \\ u_1 & 0 & \frac{\omega_o L}{2} \\ u_2 & -\frac{\omega_o L}{2} & 0 \end{bmatrix} \frac{\partial H}{\partial \mathbf{x}} - \begin{bmatrix} CI_o\sqrt{2x_1} & 0 & 0 \\ 0 & r/2 & 0 \\ 0 & 0 & r/2 \end{bmatrix} \frac{\partial H}{\partial \mathbf{x}} + \begin{bmatrix} 0 \\ 0 \\ -\frac{E}{2} \end{bmatrix}. \tag{38}$$

Or in a more compact form

$$\dot{\mathbf{x}} = [\mathbf{J}(\mathbf{u}) - \mathbf{R}(\mathbf{x})] \frac{\partial H}{\partial \mathbf{x}}(\mathbf{x}) + \mathbf{g}, \tag{39}$$

where $\mathbf{J} = -\mathbf{J}^T$, $\mathbf{R}(\mathbf{x}) = \mathbf{R}^T(\mathbf{x}) \geqslant 0$ are the interconnection and damping matrices, respectively, and vector $\mathbf{g}$ models an external disturbance. Note that $H(x)$ is the DC-component of the Hamiltonian $H_T(z)$ in equation (27); i.e.

$$H(\mathbf{x}) = \langle H_T(z)\rangle_0 = \frac{1}{C}\langle z_2\rangle_0 + \frac{1}{L}\langle\phi\rangle_1^{R^2} + \frac{1}{L}\langle\phi\rangle_1^{I^2} \tag{40}$$

or

$$H(\mathbf{x}) = \frac{1}{C}x_1 + \frac{1}{L}x_2^2 + \frac{1}{L}x_3^2. \tag{41}$$

The GSSA system in equation (38) preserves the PCH structure of the system in equation (28), with the remarkable advantage of a regulation control objective. This allows the IDA passivity based design approach to be methodically used. In this line, an IDA-PB control fulfilling system specifications is designed in the next section. The control law depends on the output voltage DC-component and requires measuring the DC output current to guarantee robustness with respect to load variations.

2.5 Controller design

The final objective of the IDA-PBC approach [12] is to design a feedback control $\mathbf{u} = \boldsymbol{\beta}(\mathbf{x})$ such that the closed-loop dynamics is the PCH reference system:

$$\dot{\mathbf{x}} = [\mathbf{J}_d(\mathbf{x}) - \mathbf{R}_d(\mathbf{x})] \frac{\partial H_d}{\partial \mathbf{x}}(\mathbf{x}), \tag{42}$$

where $\mathbf{J}_d(\mathbf{x}) = -\mathbf{J}_d^T(\mathbf{x})$ and $\mathbf{R}_d(\mathbf{x}) = \mathbf{R}_d^T(\mathbf{x}) \geqslant 0$ are targeted interconnection and damping matrices, and the new energy function $H_d(\mathbf{x}) = H(\mathbf{x}) + H_a(\mathbf{x})$ has a strict local minimum at the desired equilibrium.

Following [12], we proceed in the standard manner.

(i) (Structure preservation) Given $\mathbf{J}_d(\mathbf{x})$ and $\mathbf{R}_d(\mathbf{x})$, let $\mathbf{J}_a(\mathbf{x})$ and $\mathbf{R}_a(\mathbf{x})$ be defined by

$$\begin{aligned} \mathbf{J}_d(\mathbf{x}) &:= \mathbf{J}(\mathbf{x}, \boldsymbol{\beta}(\mathbf{x})) + \mathbf{J}_a(\mathbf{x}) = -\left[\mathbf{J}(\mathbf{x}, \boldsymbol{\beta}(\mathbf{x})) + \mathbf{J}_a(\mathbf{x})\right]^T, \\ \mathbf{R}_d(\mathbf{x}) &:= \mathbf{R}(\mathbf{x}) + \mathbf{R}_a(\mathbf{x}) = \left[\mathbf{R}(\mathbf{x}) + \mathbf{R}_a(\mathbf{x})\right]^T \geqslant 0. \end{aligned}$$

Then, the desired dynamics is achieved if it is possible to find functions $\boldsymbol{\beta}(\mathbf{x})$ and $\mathbf{k}(\mathbf{x}) := \frac{\partial H_a(\mathbf{x})}{\partial \mathbf{x}}$ satisfying

$$\left[\mathbf{J}(\mathbf{x}, \boldsymbol{\beta}(\mathbf{x})) + \mathbf{J}_a(\mathbf{x}) - (\mathbf{R}(\mathbf{x}) + \mathbf{R}_a(\mathbf{x}))\right] \mathbf{k}(\mathbf{x}) = -\left[\mathbf{J}_a(\mathbf{x}) - \mathbf{R}_a(\mathbf{x})\right] \frac{\partial H}{\partial \mathbf{x}}(\mathbf{x}) + \mathbf{g} \tag{43}$$

(ii) (Integrability) $\mathbf{k}(\mathbf{x})$ is the gradient of a scalar function. That is,

$$\frac{\partial k_i}{\partial x_j}(\mathbf{x}) = \frac{\partial k_j}{\partial x_i}(\mathbf{x})$$

(iii) (Equilibrium condition)

$$\frac{\partial H_d}{\partial \mathbf{x}}(\mathbf{x}^*) = 0$$

(iv) (Lyapunov Stability)

$$\left.\frac{\partial^2 H_d}{\partial x^2}\right|_{\mathbf{x}^*} > 0$$

If conditions (43), (ii), (iii) and (iv) hold, then $\mathbf{x}^*$ is a (locally) stable equilibrium point of the closed-loop system.

Let us particularise the aforementioned procedure for the full-bridge boost rectifier controller defining $\mathbf{J}_d(\mathbf{x}) = \mathbf{J}(\mathbf{x}, \boldsymbol{\beta}(\mathbf{x}))$ and $\mathbf{R}_d(\mathbf{x}) = \mathbf{R}(\mathbf{x})$, i.e. $\mathbf{J}_a(\mathbf{x}) = 0$ and $\mathbf{R_a}(\mathbf{x}) = 0$.

• (Structure Preservation)

Equation (43) yields

$$\begin{aligned} 0 &= -I_o C\sqrt{2x_1}k_1 - u_1 k_2 - u_2 k_3 && (44)\\ 0 &= u_1 k_1 - \frac{r}{2}k_2 + \frac{\omega L}{2}k_3 && (45)\\ 0 &= u_2 k_1 - \frac{\omega L}{2}k_2 - \frac{r}{2}k_3 + \frac{E}{2}. && (46) \end{aligned}$$

Then, from equations (45)-(46),

$$\left.\begin{aligned} u_1 &= -\frac{-r\,k_2 + \omega\,L\,k_3}{2\,k_1}\\ u_2 &= \frac{\omega\,L\,k_2 + r\,k_3 - E}{2\,k_1} \end{aligned}\right\}. \qquad (47)$$

• (Integrability) Replacing equation (47) in (44) and taking into account that $\mathbf{k}(\mathbf{x}) = \frac{\partial H_a(\mathbf{x})}{\partial \mathbf{x}}$, the following partial differential equation is obtained:

$$2I_o\,C\,\sqrt{2x_1}\left(\frac{\partial H_a}{\partial x_1}\right)^2 = -r\left(\frac{\partial H_a}{\partial x_2}\right)^2 - \left(r\frac{\partial H_a}{\partial x_3} - E\right)\frac{\partial H_a}{\partial x_3}. \qquad (48)$$

As we are interested in control inputs u_1, u_2, which only depend on the output voltage DC-component, we take $k_2 = k_2(x_1)$ and $k_3 = k_3(x_1)$. Then, by the integrability condition

$$\frac{\partial k_i}{\partial x_1} = \frac{\partial^2 H_a}{\partial x_1 \partial x_i} = \frac{\partial^2 H_a}{\partial x_i \partial x_1} = 0$$

for $i = 2$, 3 and $k_2 = a_2$ and $k_3 = a_3$ are indeed constant. Thus, the PDE is actually an ODE on x_1, whose solution is given by

$$H_a(\mathbf{x}) = -\frac{2}{3}\sqrt{-\frac{\sqrt{2x_1}}{I_o\,C}\,x_1\,(a_2^2\,r + a_3^2\,r - a_3\,E)} + a_2\,x_2 + a_3\,x_3 \qquad (49)$$

and

$$\mathbf{k}(\mathbf{x}) = \left[\frac{\sqrt{2}\,(a_2^2\,r + a_3^2\,r - a_3\,E)}{6\sqrt{-I_o\,C\,\sqrt{x_1}\,\sqrt{2}\,(a_2^2\,r + a_3^2\,r - a_3\,E)}} - \frac{\sqrt{-I_o\,C\,\sqrt{x_1}\,\sqrt{2}\,(a_2^2\,r + a_3^2\,r - a_3\,E)}}{3\,I_o\,C\,\sqrt{x_1}}, a_2, a_3\right]. \qquad (50)$$

• (Equilibrium assignment)
From equation (49) and the definition of H_a ($H_a = H_d - H$), the following conditions on a_2, a_3 and I_d so that $\mathbf{x}^*$, from equation (37), is a singular point of H_d are derived:

$$\begin{aligned}\frac{1}{C} + \frac{\sqrt{-2I_oC\sqrt{C^2V_d^2}(a_2^2r + a_3^2r - a_3\,E)}}{3I_oC\sqrt{C^2V_d^2}} &= \frac{\sqrt{2}(a_2^2r + a_3^2r - a_3E)}{6\sqrt{-I_oC\sqrt{C^2V_d^2}(a_2^2r + a_3^2r - a_3E)}} \\ a_2 &= 0 \\ a_3 - I_d &= 0\end{aligned}$$

This equations system has two solutions:

$$\{a_2 = 0,\, I_d = \frac{E + \sqrt{E^2 - 8\,I_o\,V_d\,r}}{2\,r},\, a_3 = I_d\}$$

and

$$\{a_2 = 0,\, I_d = \frac{E - \sqrt{E^2 - 8\,I_o\,V_d\,r}}{2\,r},\, a_3 = I_d\}.$$

Then, taking the latter solution, k_1 and the control inputs derived in equation (47) are

$$\left.\begin{aligned}k_1 &= -\frac{\sqrt{2}\sqrt{I_o^2V_dC\sqrt{2}\sqrt{x_1}}}{2I_oC\sqrt{x_1}} \\ u_1 &= -\frac{\omega L(-E + \sqrt{E^2 - 8I_oV_dr})C\sqrt{V_oV_d}}{4rV_d} \\ u_2 &= \frac{(E + \sqrt{E^2 - 8I_oV_dr})C\sqrt{V_oV_d}}{4V_d}\end{aligned}\right\},$$

where V_o denotes the output voltage DC-component $\langle v_o\rangle_0$ and $\sqrt{2x_1} = \langle q\rangle_0 = C\langle v_o\rangle_0$.
• (Lyapunov Stability)
Replacing the values[4] of k_2, k_3 and I_d into H_a and the last, in turn, into $H_d(\mathbf{x})$, the closed-loop Hamiltonian becomes

$$H_d(\mathbf{x}) = \frac{1}{6CrL}\left(42^{(3/4)}\sqrt{CV_d}x_1^{(3/4)}rL - 3x_3CLE + 3x_3CL\sqrt{E^2 - 8I_oV_dr} - 6x_1rL - 6x_2^2Cr - 6x_3^2Cr\right).$$

Since the Hessian matrix of H_d is diagonal with positive eigenvalues, $\mathbf{x}^*$, the singular point of H_d, is a local minimum. Moreover, $\mathbf{x}^*$ is an asymptotically stable equilibrium point as can be stated noticing in equation (42) that for $I_o > 0$, $\mathbf{R}_d(\mathbf{x}) = \mathbf{R}(\mathbf{x})$ is full rank, and the solution of $\frac{\partial H_d}{\partial \mathbf{x}}(\mathbf{x}) = 0$ is unique, namely $\mathbf{x} = \mathbf{x}^*$. If $I_o = 0$, then $I_d = 0$ and x_2 and x_3 converge to zero; then, $u_2 = \frac{E}{2}\,C\sqrt{\frac{V_o}{V_d}}$. Replacing this in equation (38) yields $\frac{dx_3(t)}{dt} = 0$ if and only if $V_o = V_d$.

2.6 Simulation results

2.6.1 Linear Load

The whole system behaviour is simulated as a discrete control system using *MatLab* and *Simulink*. The continuous IDA-PB controller is discretised and implemented through a PWM so that the

[4]Note that taking $I_o = \frac{V_d}{R}$, the I_d value obtained in equation (32) is recovered.

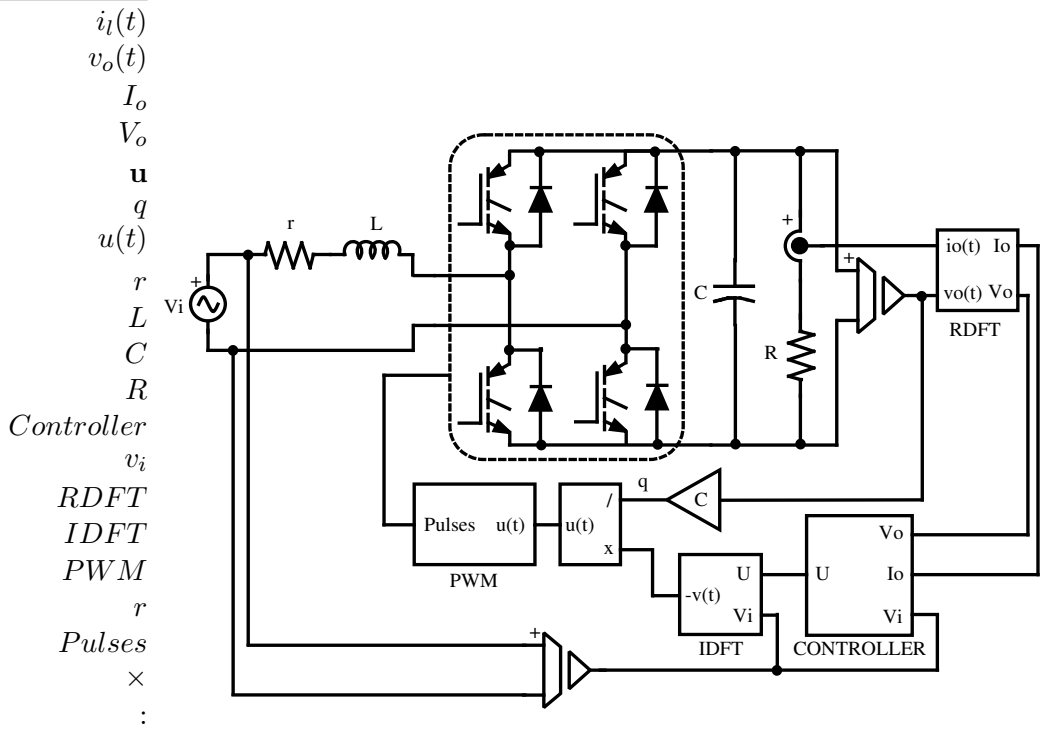

Figure 9: General Controller Scheme

simulations are closer to the actual system. fig. 9 outlines the closed-loop diagram. The actual rectifier is shown at the top of the figure with *Pulses* as the input signal and the couple $i_l(t)$ and $v_o(t)$ as the output measured variables; note that the input voltage $v_i(t)$ is sensed too for being used as input in the *Controller* and *IDFT* blocks. The real-time discrete Fourier transform is carried out in the *RDFT* block. It is based on a recursive discrete Fourier transform technique, see [6] for details, which allows the right Fourier coefficients to be obtained at sampling times. The *Controller* block computes the suitable averaged Fourier components for the control signal $\mathbf{u}(t)$ while the inverse discrete Fourier transform is performed in the *IDFT* block to obtain the discrete $v(kT)$ control signal. finally, the fixed frequency pulses are provided by the PWM block by pulse-width modulating the real valued $u(t)$ control signal.

The following parameters are used for simulation purposes: $R_{\text{nom}} = 100\ \Omega$, $L = 2$ mH, $C = 2200\ \mu$F, $E = 120$ V, $f = 50$ Hz, $V_d = 200$ V; the PWM switching frequency is $f_s = 20$KHz.

The obtained output voltage for the three values of the load, i.e. $R = R_{\text{nom}} = 100\ \Omega$ for $0\text{s} \leqslant t < 0.5\text{s}$, $R = 20\ \Omega$ for $0.5\text{s} \leqslant t < 1\text{s}$, and $R = 500\ \Omega$ for $1\text{s} \leqslant t < 1.5\text{s}$, is depicted in figure 10. The inductor current $i(t)$ and the scaled input voltage $v_i(t)$ are depicted in figure 11 for each of the selected loads. These figures show that the specifications are fulfilled.

2.6.2 NonLinear Load

Using averaged sensed variables instead of actual ones lets this controller to deal with nonlinear loads. To this end, simulation of this kind of load has been considered by means of resistance values composed by a mean value plus a triangular ripple (20% amplitude) at the fundamental frequency. Fig. 12 shows the output DC voltage regulation performance and Fig. 13 shows the power factor correction performance for the case of a nonlinear load which mean values change from 100Ω to 50Ω and from the later to 500Ω.

2.7 Experimental Setup and Results

The experimental setup used to test the designed controller has the following parts:

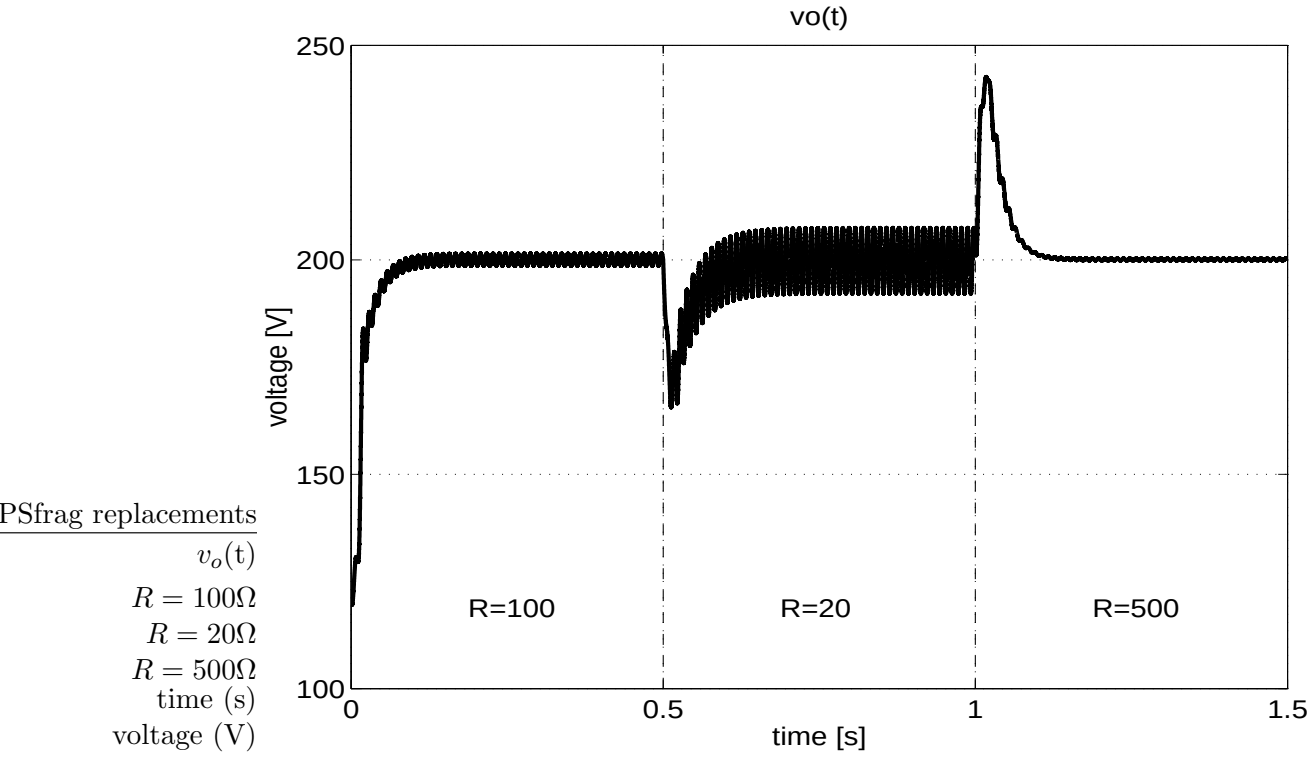

Figure 10: Time evolution of DC output voltage, $v_o(t)$, in front of load changes.

- Full-bridge boost converter with IGBT switches (1200 V, 100 A) and parameters: $r = 0.092\Omega$, $L = 2.7$mH, $C = 1400\mu$F. The switching frequency of the converter is 20 KHz and a synchronous centered-pulse single-update pulse-width modulation strategy is used to map the controller's output to the IGBT gate signals.

- Load: resistive load bank which allows to select $R = 513\Omega$, $R = 120\Omega$, $R = 60\Omega$ or open circuit.

- Analog circuitry of sensors: the AC mains voltage, and DC bus voltage are sensed with isolation amplifiers whereas load current is sensed with an hall-effect sensor. All the signals from the sensors pass through the corresponding gain conditioning stages to adapt their values to A/D converters.

- Control hardware and DSP implementation: the control algorithm has been implemented using the Analog Devices single-chip DSP motor controller ADMC401 processor. The processing core of this device is the 26MHz fixed-point ADSP-2171 DSP processor. The ADMC401 deals with the PWM generation and the A/D conversions. The sampling rate of the A/D channels is $T_s = 20$Khz, the same as the switching frequency of the Full-Bridge system.

- The nominal RMS AC mains voltage is $V_s = 48.9$V RMS and its nominal frequency is 50 Hz.

- Control Objectives: The desired regulated DC output voltage and the power factor should be $V_o = 130$V and near unity, respectively. It is important to note that the IGBT switches are oversized for this particular application resulting in undesirable power losses and harmonic distortion. These power looses has been taken into account increasing the series

PSfrag replacements
$i(t)$ and v_i(t)
$v_i(t)$
$i(t)$
time (s)

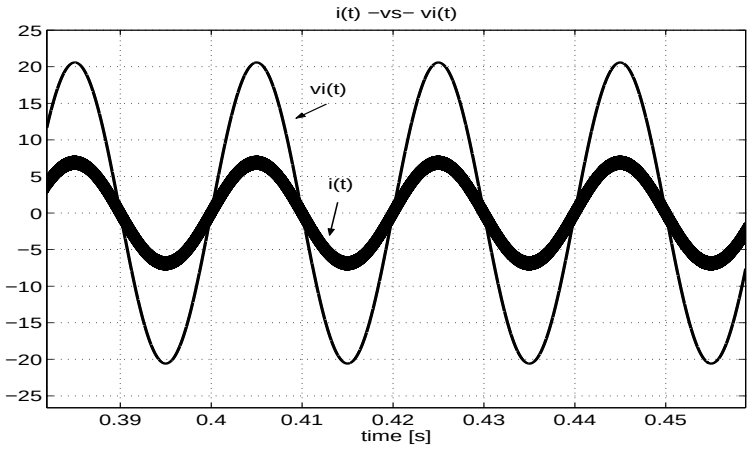

(a) $R = Rn = 100\Omega$

PSfrag replacements
$i(t)$ and v_i(t)
$v_i(t)$
$i(t)$
time (s)

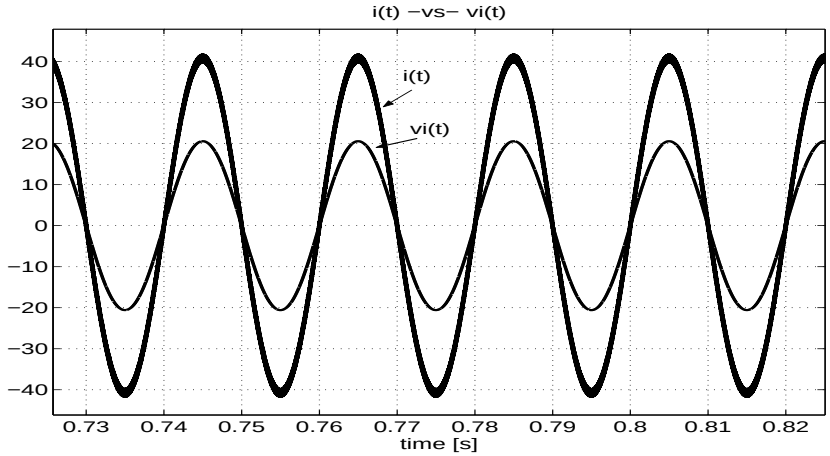

(b) $R = 20\Omega$

PSfrag replacements
$i(t)$ and v_i(t)
$v_i(t)$
$i(t)$
time (s)

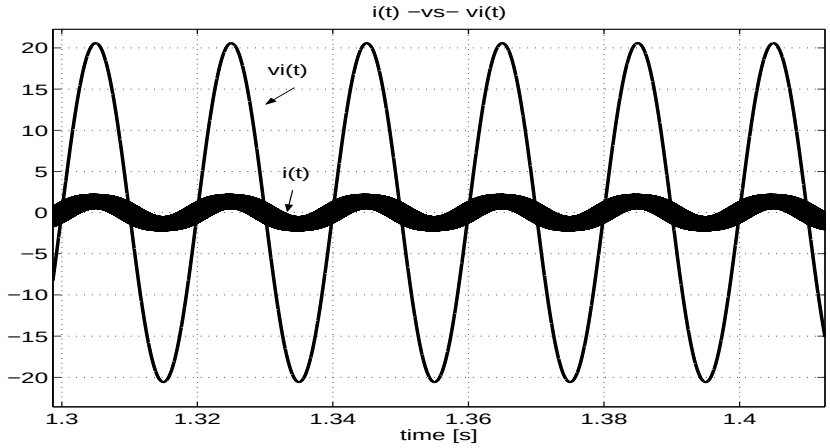

(c) $R = 500\Omega$

Figure 11: $i(t)$ and scaled $v_i(t)$: a) nominal load $R = 100\Omega$, b) $R = 20\Omega$, c) $R = 50\Omega$.

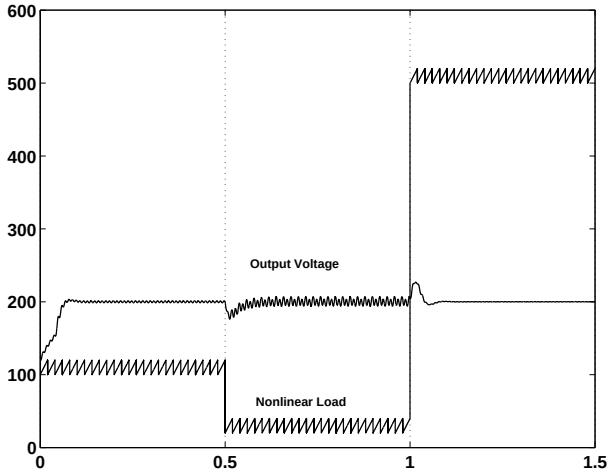

Figure 12: DC bus voltage (V_o) and nonlinear load resistance (R) values.

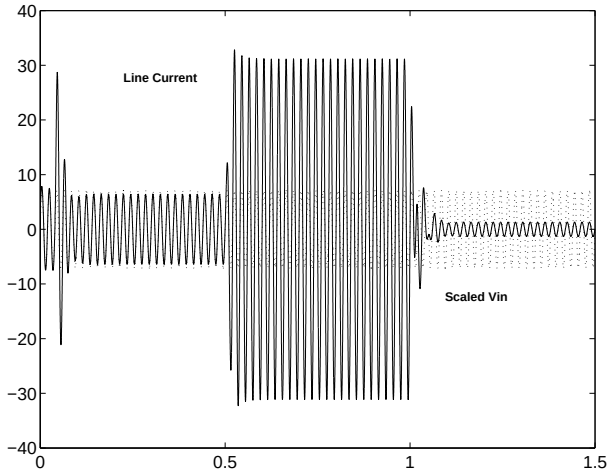

Figure 13: Source voltage v_i and line current i_l

resistance r by a switch looses resistance of $rsw = 0.3\Omega$. The system performance could be improved replacing these IGBT switches with low power ones.

From the aforementioned experimental setup some results have been obtained with the designed digital controller. These results are presented through oscilloscope and power analyzer screen dumps of the AC mains electrical variables and, as appropriate, the DC bus voltage.

2.7.1 DC bus voltage regulation

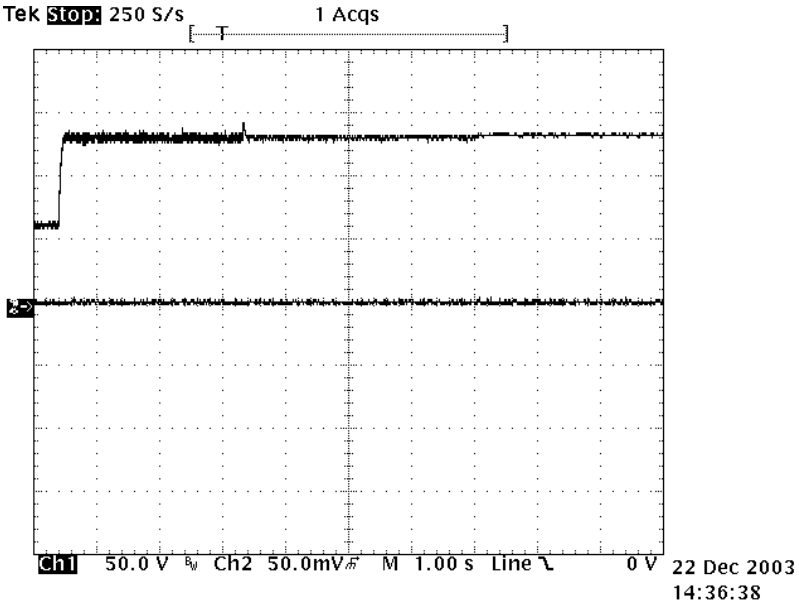

Figure 14: DC bus voltage (V_o) in front of load variations (1 sec./time-division).

In this experiment, at start time the DC bus voltage rests at the diode rectifier level with a resistive load of $R = 60\Omega$. Then, the control action is applied keeping the load resistance and the output voltage increases to the desired DC value. Afterwards, two load changes from $R = 60\Omega$ to $R = 120\Omega$ and from $R = 120\Omega$ to no-load condition were applied at $t = 3.3$ and $t = 7.0$ seconds, respectively. Fig. 14 shows the shape of the DC bus output voltage. As it can be seen, the controlled system is robust with respect to load variations.

2.7.2 Line current and power factor behaviour

This subsection shows, in Fig. **??** and Fig. **??**, the line current shape and power factor value for two load conditions, namely $R = 60\Omega$ and $R = 120\Omega$. As it can be seen, the higher the power managed, the closer to unity the power factor is. It is important to remark that the $\cos(\phi)$ is equal to one in both cases.

2.8 Conclusions

This paper shows how the GSSA modelling technique can be used not only to accurately model the behaviour of variables in an AC-DC full-bridge power electronic converter, but also to explore advanced control techniques taking advantage of the inherent domain change, from time to GSSA domain.

In the case considered here, a non-standard tracking control problem for a full-bridge boost rectifier results in a regulation one. An IDA-PB control has been designed measuring the load

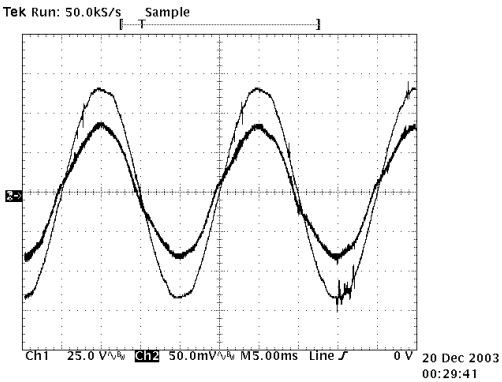

(a) CH1: v_i V, CH2: i_l10mV/A

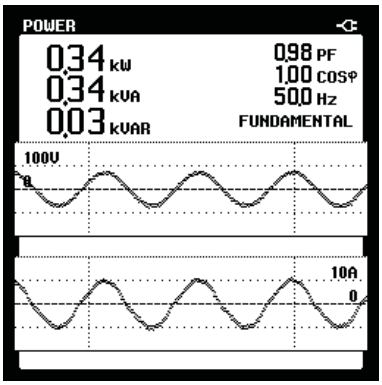

(b) Power input Data

Figure 15: Source voltage and line current, and power information at AC mains for $R = 60\Omega$

current and the load voltage, and presuming the input voltage is known. The closed-loop system is robust to load variations achieving unity power factor in the AC mains and load voltage regulation. Some experimental results are included showing the the feasibility of the designed controller.

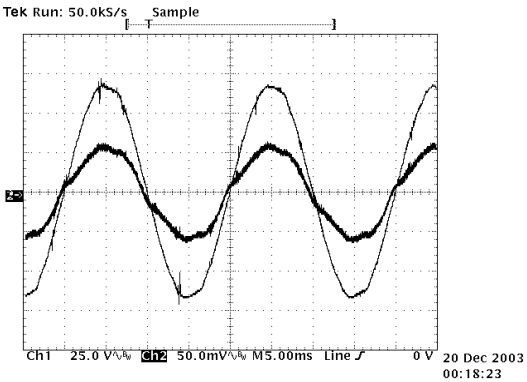

(a) CH1: v_i V, CH2: i_l10mV/A

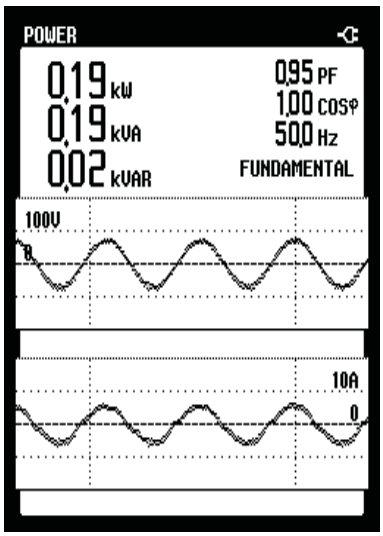

(b) Power input Data

Figure 16: Source voltage and line current, and power information at AC mains for $R = 120\Omega$

References

[1] J. T. Boys and A. W. Green. Current-forced single-phase reversible rectifier. *IEE Proc. B*, 136:205–211, 1989.

[2] V. Caliscan, G. Verghese, and A. Stanković. Multi-frequency averaging of dc/dc converters. *IEEE Trans. on Power Electronics*, 14(1):124–133, January 1999.

[3] D. Lee, G. Lee, and K. Lee. Dc-bus voltage control of three-phase ac/dc pwm converters using feedback linearization. *IEEE Trans. on Industry Applications*, 36(3):826–832, May/June 2000.

[4] G. Escobar, D. Chevreau, R. Ortega, and E. Mendes. An adaptive passivity-based controller for a unity power factor rectifier. *IEEE Trans. on Control Systems Technology*, 9(4):637–644, July 2001.

[5] R. Griñó, E. Fossas, and D. Biel. Sliding mode control of a full-bridge unity power factor rectifier. *A. Zinober and D. Owens (Eds.): Nonlinear and Adaptive Control, LNCIS 281*, pages 139–148, November 2001.

[6] J. Rosendo and A. Gómez. Efficient moving-window dft algorithms. *Circuits and Systems II: Analog and Digital Signal Processing, IEEE Transactions on*, 45:256–260, February 1998.

[7] B. Lin and H. Lu. Single-phase power-factor-correction ac/dc converters with three pwm control schemes. *IEEE Trans. on Aerospace and Electronic Systems*, 36:189–200, January 2000.

[8] J. Mahdavi, A. Emaadi, M. Bellar, and M. Ehsani. Analysis of power electronic converters using the generalized state-space averaging approach. *IEEE Trans. on Circuits and Systems I*, 44(8):767–770, August 1997.

[9] N. Mohan, T. M. Undeland, and W. P. Robbins. *Power Electronics. Converters,Applications, and Design.* John Wiley & Sons, 1995.

[10] O. García, J. Cobos, R. Prieto, P. Alou, and J. Uceda. Power factor correction: A survey. *IEEE 32nd Annual Power Electronics Specialists Conference, PESC. 2001*, 1:8–13, 2001.

[11] R. Morici, C. Rossi, and A. Tonielli. Variable structure controller for ac/dc boost converter. *IEEE. 20th International Conference on Industrial Electronics, Control and Instrumentation*, 3:1449–1454, 1994.

[12] R. Ortega, A. Schaft, B. Maschke, and G. Escobar. Interconnection and damping assigment passivity-based control of port-controlled hamiltonian systems. *Automatica*, 38:585–596, April 2002.

[13] S. Sanders, J. Noworolski, X. Liu, and G. Verghese. Generalized averaging method for power conversion systems. *IEEE Trans. on Power Electronics*, 6:251–259, April 1991.

[14] H. Sira-Ramirez. Sliding motions in bilinear switched networks. *IEEE Trans. on Circuit and Systems*, (34):919–933, 1987.

[15] V. I. Utkin. *Sliding Modes and their Applications in Variable Structure Systems.* Mir, Moscow, 1978.

[16] E. Wernekinck, A. Kawamura, and R. Hoft. A high frequency ac/dc converter with unity power factor and minumum harmonic distortion. *IEEE Trans. on Power Electronics*, (6):364–370, 1991.